COMPUTATION OF ICE BOREHOLE CLOSURE BY THE FINITE ELEMENT METHOD

Fucheng Li and Bruce Koci

Polar Ice Coring Office
University of Alaska Fairbanks
Fairbanks, Alaska 99775-1710

PICO
TR-92-1

January 1992

TABLE OF CONTENTS

LIST OF FIGURES

ACKNOWLEDGMENTS

We would like to express our sincere appreciation to Dr. John Kelley, Director of the Polar Ice Coring Office, and Mr. Kerry Stanford, Manager of the Engineering Division, Polar Ice Coring Office, for their support and encouragement on this project. We offer our sincere thanks to Dr. Viktor Zagorodnov for his kindly supply of information related to this project.

Thanks are also given to the staff of the Polar Ice Coring Office, University of Alaska Fairbanks, for their kind assistance.

The research described herein was funded by the U.S. National Science Foundation and the University of Alaska Fairbanks through the Polar Ice Coring Office and was greatly appreciated.

ABSTRACT

The ice borehole closure may affect the drilling operation when the closure rate reaches some critical level. It is essential to estimate the closure rate of ice boreholes for drilling program planning. To examine Nye's formula and to obtain more accurate estimates of ice borehole closure to various ice conditions, a finite element modeling was used. The ice was treated as non-linear visco-incompressible fluid. Glen's ice flow power law was used. The effects of change in ice density and temperature versus depth were considered. Computation was carried out by the direct iteration method.

Tests with Nye's formula show that the model can give quite accurate results in closure rate, strain rate and stresses with errors at the 4th digit number in strain rate. Nye's formula gives more conservative values. Tests with field measurements show that the exponent of power law should be considered as a variable of ice-effective stresses to get more accurate results. An empirical relation between the exponent and effective stress was obtained by modeling with field measurements. Ice density variation has small effect on the ice closure rate, while a temperature increase of 15°C may lead to 8 times the increase in the closure rate at the 1,500-m depth. Borehole diameters have a linear effect on the closure rate. Modeling results also show that the ice bottom boundary conditions can only affect borehole closure rate within, at most, 50 m from the bottom, and the effect decreases quickly within 5 m from the bottom. The ice flow has little effect on the ice borehole closure.

1. INTRODUCTION

Ice boreholes are drilled into glaciers or the ice sheet from time to time in order to study the internal structure of the ice and its movements. Unless they are artificially supported, these boreholes gradually close up under the pressure of the overlying ice. Some drilling projects in Greenland and in Antarctica require boreholes in deep, cold ice which must be maintained open for a period of hours or days to allow instruments to be lowered to the ice sheet bed. Therefore, it is important to know the ice borehole closure rate for designing the borehole diameter to be drilled.

The only analytical formula available for estimating ice borehole closure is Nye's solution (1953) to an infinite long hole subjecting uniform surface pressure. Actual ice borehole closures are caused by the overlying ice body force. For a liquid-filled ice borehole, the hole surface subjects no uniform vertical pressure. Moreover, the ice sheet bottom may be frozen onto the rock bed which must have some effect on the ice borehole closure. A compressed ice flow might also have some effect on the borehole closure. What the difference might be with Nye's formula to these real ice conditions remains unknown.

Numerical modeling is a powerful method for studying ice creep on both a large and a small scale. Typically, the finite element method can be used to model the ice borehole closure with a suitable rheological law for polycrystalline ice. Many suggestions on ice-flow law have been made based on laboratory experiments and field measurements. It is possible to get reasonable estimates of ice borehole closure by a finite element method.

The purpose of the study presented here is to examine Nye's formula with real ice borehole conditions and to try to give more accurate estimates of ice borehole closure rates. The next section of this report describes the basic methods used in the computation method. Test results and applications of the modeling program are illustrated in Sections 3 and 4, respectively. Conclusions are given in Section 5.

2. METHOD OF COMPUTATION

Calculations were carried out with a computer program modified by the authors based on a finite element code for plane viscous incompressible fluid problems. To consider the nonlinear rheological properties of ice, direct iteration methods were used to solve the global equations and to calculate element stresses.

2.1 Flow Law of Ice

The basic postulate is that polycrystalline ice is an incompressible, nonlinear viscous fluid. Experiments by Rigsby (1957) demonstrated that hydrostatic pressure does not affect the flow law, which is justification for treating ice as incompressible (Hutter, 1983). Thus stress tensor σ_{ij} can be written as

$$\sigma_{ij} = -p\delta_{ij} + \sigma'_{ij}, \tag{2.1}$$

where p is called hydrostatic pressure, which produces no change of shape; σ'_{ij} is the deviatoric stress tensor which produces no change of volume, and $\delta_{ij}=1$, if $i=j$ or $\delta_{ij}=0$ if $i\neq j$.

For Newtonian fluids, there is a linear relationship between deviatoric stress and strain rate as:

$$\sigma'_{ij} = (1 + \delta_{ij})\mu\dot{\varepsilon}_{ij}, \tag{2.2}$$

where μ is the viscosity coefficient, $\dot{\varepsilon}_{ij}$ is the strain rate tensor. While under a long-term, stable load, ice flow may be considered to be in the secondary creep process. It usually has a nonlinear stress-strain rate relationship under a high stress state as typically presented by Glen (1955):

$$\dot{\varepsilon}_{ij} = A\tau^{n-1}\sigma'_{ij}, \tag{2.3}$$

where τ is effective stress, given by

$$2\tau^2 = \sigma'_{ij}\sigma'_{ij}. \tag{2.4}$$

The exponent n in (2.3) varies from 2 to 4 (Hutter, 1983) with a mean of about 3. So n is usually taken as a constant, and $n=3$ is adopted for normally encountered glaciers and ice sheets (Paterson, 1981). Details about n used in this model will be disscussed in the next section. Coefficient A in (2.3) depends on ice temperature, crystal size and orientation, impurity content and possibly other factors. It varies with the absolute temperature T according to the Arrhenius relation

$$A = A_o exp(\frac{-Q}{RT}). \tag{2.5}$$

where R is the gas constant (8.314 *J/mol/°* K), Q is the activation energy for creep and A_0 is a constant. Paterson (1981) gave values of

$$A_o = 4.2 \times 10^{-13}/s.Pa^3. \quad Q = 6 \times 10^4 J/mol. \quad for \quad T \leq -10°C \tag{2.6}$$

$$A_o = 2.0 \times 10^3/s.Pa^3. \quad Q = 1.39 \times 10^5 J/mol. \quad for \quad T > -10°C. \tag{2.7}$$

Considering (2.2), (2.3) may be written in the form of

$$\sigma'_{ij} = 2\mu\dot{\varepsilon}_{ij} \tag{2.8}$$

with

$$\mu = \frac{1}{2A\tau^{n-1}}. \tag{2.9}$$

(2.3) through (2.9) were used in the modeling. Direct iterative methods were used in solving the global equations and calculating stresses. In each iteration process, the nonlinear relation (2.3) was treated linearly with (2.8) and (2.9).

2.2 Basic Equations

The ice borehole was modeled as an axisymmetric cylinder with a centered symmetric axis Z (Fig. 1).

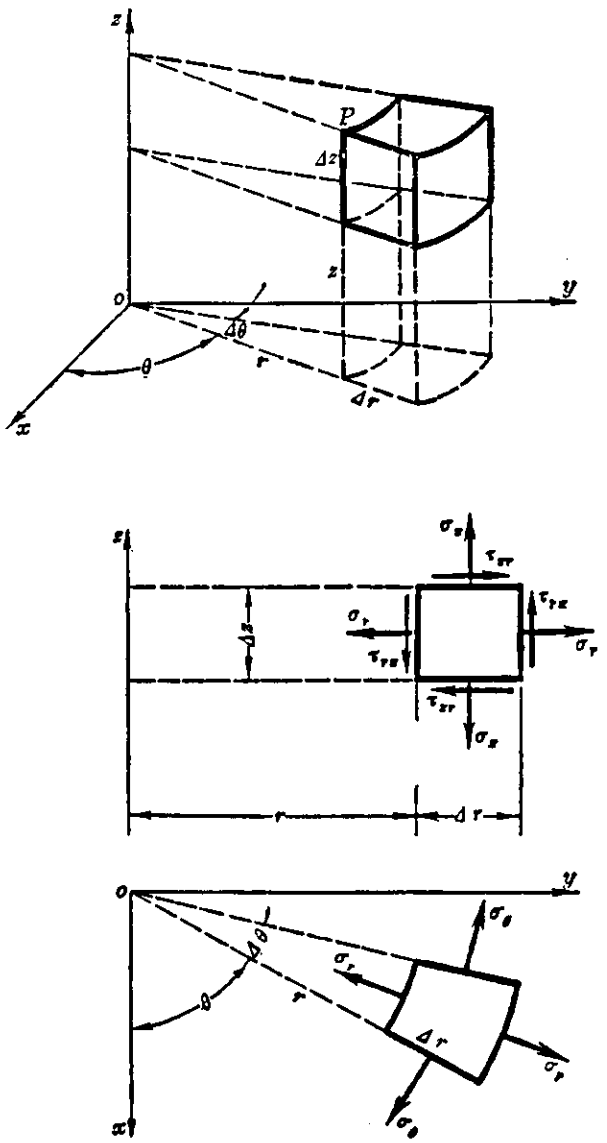

Figure 1. Axisymmetric cylindrical modeling coordinate system

In cylindrical coordinates, the deviatoric stress vector $\{\sigma'\}$ can be written as

$$\left\{\sigma'\right\} = \begin{Bmatrix} \sigma'_r \\ \sigma'_\theta \\ \sigma'_z \\ \tau'_{zr} \end{Bmatrix} = \begin{Bmatrix} 2\mu\dot{\varepsilon}_r \\ 2\mu\dot{\varepsilon}_\theta \\ 2\mu\dot{\varepsilon}_z \\ 2\mu\dot{\gamma}_{rz} \end{Bmatrix}. \tag{2.10}$$

where σ'_r, σ'_θ, σ'_z are normal stresses in the principal directions of radial, circumferential and axial, respectively, and τ'_{zr} is shear stress. The strain rate vector $\{\dot{\varepsilon}\}$ can be expressed in partial velocities $\{U\}$ as

$$\{\dot{\varepsilon}\} = \begin{Bmatrix} \dot{\varepsilon}_r \\ \dot{\varepsilon}_\theta \\ \dot{\varepsilon}_z \\ \dot{r}_{zr} \end{Bmatrix} = \begin{Bmatrix} \frac{\partial u}{\partial r} \\ \frac{u}{r} \\ \frac{\partial w}{\partial z} \\ \frac{\partial u}{\partial z} + \frac{\partial w}{\partial r} \end{Bmatrix}, \tag{2.11}$$

where $\dot{\varepsilon}_r$, $\dot{\varepsilon}_\theta$ and $\dot{\varepsilon}_z$ are normal strain rates, $\dot{r}_r$ is shear strain rate. u, w are velocities along R, Z axes, respectively. From (2.10)

$$\{\sigma'\} = 2\mu \begin{bmatrix} 1 & & & \\ & 1 & & 0 \\ & & 1 & \\ 0 & & & 1 \end{bmatrix} \{\dot{\varepsilon}\} = 2\mu I\{\dot{\varepsilon}\}, \tag{2.12}$$

where

$$\mu = \frac{1}{2A\bar{\tau}^{n-1}}. \tag{2.13}$$

and I is the unit matrix,

$$I = \begin{bmatrix} 1 & & & \\ & 1 & & 0 \\ & & 1 & \\ 0 & & & 1 \end{bmatrix}. \tag{2.14}$$

To consider the incompressibility in the finite element formulation, a penalty method (Cuvelier and Segal, 1986) was used, which may also reduce computing time and memory. In the penalty method the continuity equation is perturbed with a small number α times the pressure p:

$$\alpha p + div\vec{u} = 0. \tag{2.15}$$

It can be written as

$$p = -\frac{1}{\alpha} div\vec{u} = -\lambda div\vec{u}. \tag{2.16}$$

where $\lambda = 1/\alpha$ is called the penalty number. Thus

$$-p = \lambda(\dot{\varepsilon}_r + \dot{\varepsilon}_\theta + \dot{\varepsilon}_z) = \lambda[1. \quad 1. \quad 1. \quad 0]\{\dot{\varepsilon}\} = \lambda D\{\dot{\varepsilon}\}, \tag{2.17}$$

where

$$D = [1. \quad 1. \quad 1. \quad 0]. \tag{2.18}$$

To avoid ill-conditioning of global equations and numerical difficulty, the penalty number λ was chosen 10^8 in double precision (Cook *et al.*, 1989).

A four-node, isoparametric circle element (Fig. 2) was used. The element shape functions are

$$N_i = \frac{1}{4}(1 + \xi_i)(1 + \eta_i). \qquad (i = 1, 2, 3, 4) \tag{2.19}$$

where

$$\xi_i = \begin{cases} -\xi. & \text{i=1,4} \\ \xi. & \text{i=2,3} \end{cases}, \quad and \quad \eta_i = \begin{cases} -\eta. & \text{i=1,2} \\ \eta. & \text{i=3,4} \end{cases}. \tag{2.20}$$

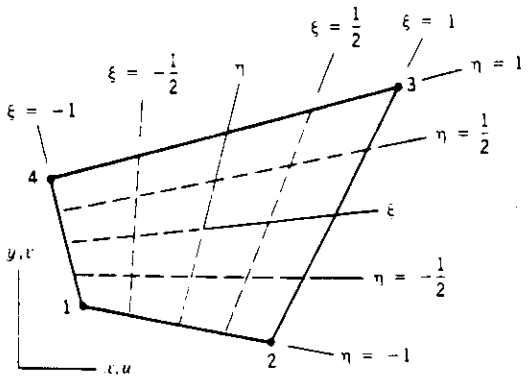

(a) Four-node plane isoparametric element in xy space.

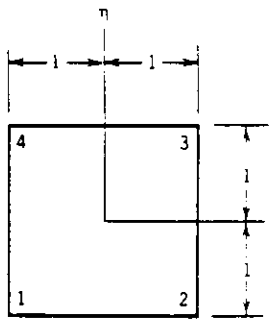

(b) Plane isoparametric element in $\xi\eta$ space.

Figure 2. Element coordinate system.

Strain rate-velocity matrix

$$[B] = [B_1, \quad B_2, \quad B_3, \quad B_4], \tag{2.21}$$

with

$$B_i = \begin{bmatrix} \frac{\partial N_i}{\partial r} & \frac{N_i}{r} & 0 & \frac{\partial N_i}{\partial z} \\ 0 & 0 & \frac{\partial N_i}{\partial z} & \frac{\partial N_i}{\partial r} \end{bmatrix}^T, \quad (i = 1, 2, 3, 4) \tag{2.22}$$

Then

$$\{\dot{\varepsilon}\} = [B]\{u\}. \tag{2.23}$$

where

$$\{u\} = [u_1, \quad w_1, \quad u_2, \quad w_2, \quad u_3, \quad w_3, \quad u_4, \quad w_4]^T. \tag{2.24}$$

The element stiffness matrix is

$$[k]^e = 2\pi \int_{-1}^{1} \int_{-1}^{1} (\lambda B^T D B + 2\mu B^T B)|J| r \, d\xi \, d\eta. \tag{2.25}$$

where $|J|$ is the determinant of the Jacobian matrix:

$$|J| = \begin{bmatrix} \frac{\partial r}{\partial \xi} & \frac{\partial z}{\partial \xi} \\ \frac{\partial r}{\partial \eta} & \frac{\partial z}{\partial \eta} \end{bmatrix}. \tag{2.26}$$

For rectangular elements the consistent element nodal loads caused by body forces can be computed as for no-isoparametric elements.

2.3 Computation Flowchart

The direct iterative methods were used in solving the global equations and in computing element stresses. As a first step, all μs in each element stiffness matrix were arbitrarily set equal to a constant, e.g., 1. After assembling the global stiffness matrix, each element strain rate was found by solving the global equations. Then the stresses for each element were determined by (2.3) with an iteration scheme: in the first step $\mu_{(1)} = \frac{1}{2A\tau^{n-1}_{(1)}} = 1$, then the stress deviators $\sigma'_{ij(1)}$ were found. With these new $\sigma'_{ij(1)}$, $\tau_{(i+1)}$ was calculated with (2.4) and $\mu_{(i+1)}$ was obtained by

$$\mu_{(i+1)} = 0.5(\mu_{(i)} + \frac{1}{2A\tau^{n-1}_{(i+1)}}), \tag{2.27}$$

and so on. This procedure was repeated until $|\mu_{(i)}-\mu_{(i+1)}| / \mu_{(i)} \leqq 0.05$. The global stiffness matrix elements were replaced by each new element stiffness matrix with its final iteration $\mu_{(i+1)}$. After all the element stiffness values were replaced in the global matrix, the solving procedure was repeated. This global equation-solving iteration was continued until each element iteration number $\nrightarrow 1$.

The computation flowchart is shown in Figure 3.

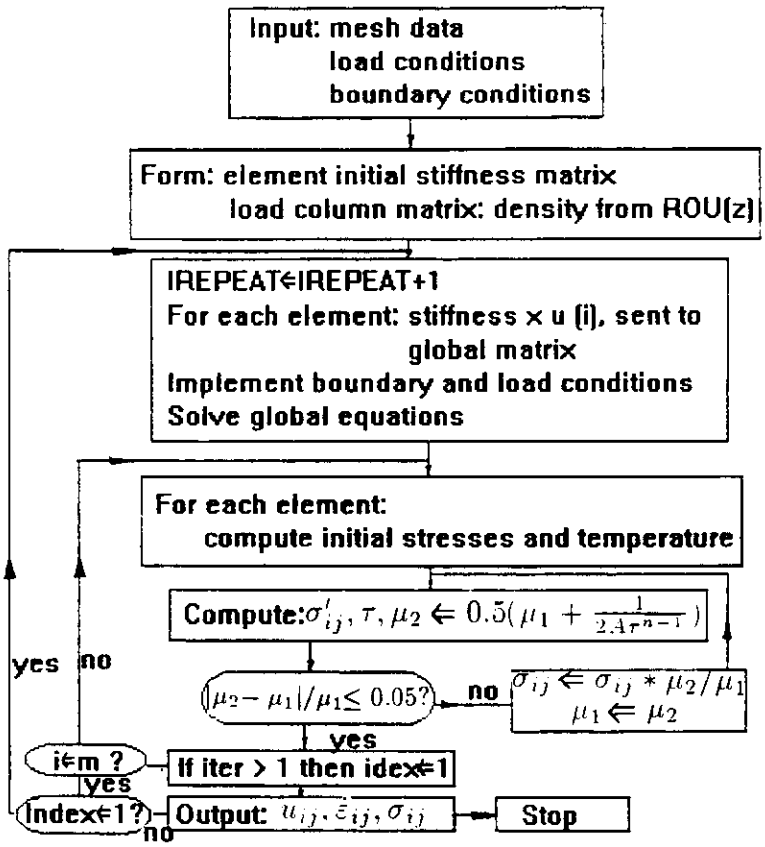

Figure 3. Computation flowchart of ice borehole closure modeling.

3. TESTS OF THE NUMERICAL MODEL

To examine this numerical model, both theoretical analysis results and field measurement data were used to compare with modeling results. As mentioned in Section 2, the exponent n has a wide range from 1.5 to 4.2. This may be sensitive to the model results. So n was determined by examining two field measurements: 1) Gow's data (1963) from a dry-ice borehole at Byrd Station, Antarctica; and 2) data of Hansen and Gundestrup (1988) as well as Gundestrup and Hansen (1984) from a liquid-filled ice borehole at Dye 3, south Greenland.

3.1 Tests with Nye's Formula

For an infinite long cylindrical hole with uniform tension q applied to the hole surface radially, the radial strain rate at the hole surface is given by Nye's formula (1953):

$$\dot{\varepsilon}_a = -\frac{u_a}{a} = A(\frac{q}{n})^n, \tag{3.1}$$

where a is the hole radius; u_a is the hole closure rate at the hole surface; A and n have the same meaning as in (2.3) which means (2.3) is applicable to this solution. The closure rate at the hole surface is

$$u_a = -aA(\frac{q}{n})^n. \tag{3.2}$$

Nye also gave relative strain rate and relative radial stress as:

$$\left(\frac{\dot{\varepsilon}_r}{\dot{\varepsilon}_a}\right) = \left(\frac{a}{r}\right)^2 \tag{3.3}$$

and

$$\left(\frac{\sigma_r}{q}\right) = \left(\frac{a}{r}\right)^{\frac{2}{n}}, \tag{3.4}$$

where r denotes radius of a spot in the hole wall, $\dot{\varepsilon}_r$ and σ_r are strain rate and radial stress at the spot. The assumptions for this analytical solution include: 1) zero strain rate in the hole axis direction, *i.e.*, $\dot{\varepsilon}_z = 0$; and 2) $\sigma'_r = \infty = 0$.

To run the computer model, a typical ice borehole was chosen with $q = 10^7 pa$, $n = 3$, $A = 2.9869 \times 10^{-25} (s^{-1} pa^{-3})$ (corresponding to -15°C) and $a = 0.05\ m$. The modeling mesh sketch is shown in Figure 4.

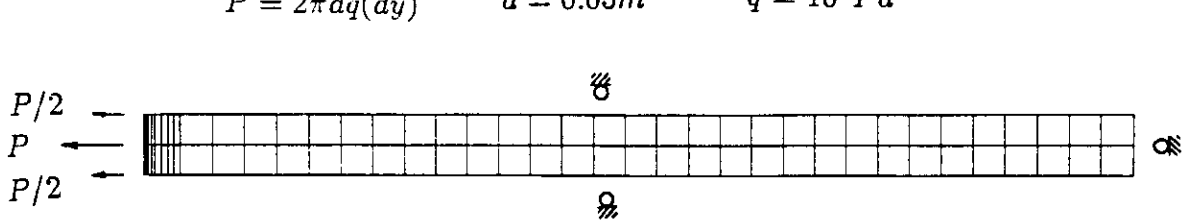

Figure 4. Sketch of modeling mesh for an idealized ice borehole. Uniform tension $q = 10^7 pa$, hole radius $a = 0.05\ m$. Consistant nodal load $p = 2\pi aq(dy)$, dy is element vertical dimension, 1 m. Horizontal dimension varies from 0.025 to 1 m. denotes boundary restriction perpendicular to the boundary.

The results of relative strain rate and closure rate by both modeling and Nye's formula are shown in Figures 5 and 6. These results show that the numerical mode can give quite accurate results as Nye's formula could, with errors at the 4th digit number in relative strain rate and the 3rd digit number in closure rate. Figure 7 shows that the relative stress from modeling is also consistant with Nye's formula results.

From Figures 6 and 7 one can see that ice borehole closure rate and stress decrease quickly as distance increases from the hole within the range of 10 times of the hole radius. Therefore, in the design of the model, the modeling mesh element dimension in the radial direction should be relative to the size of this area.

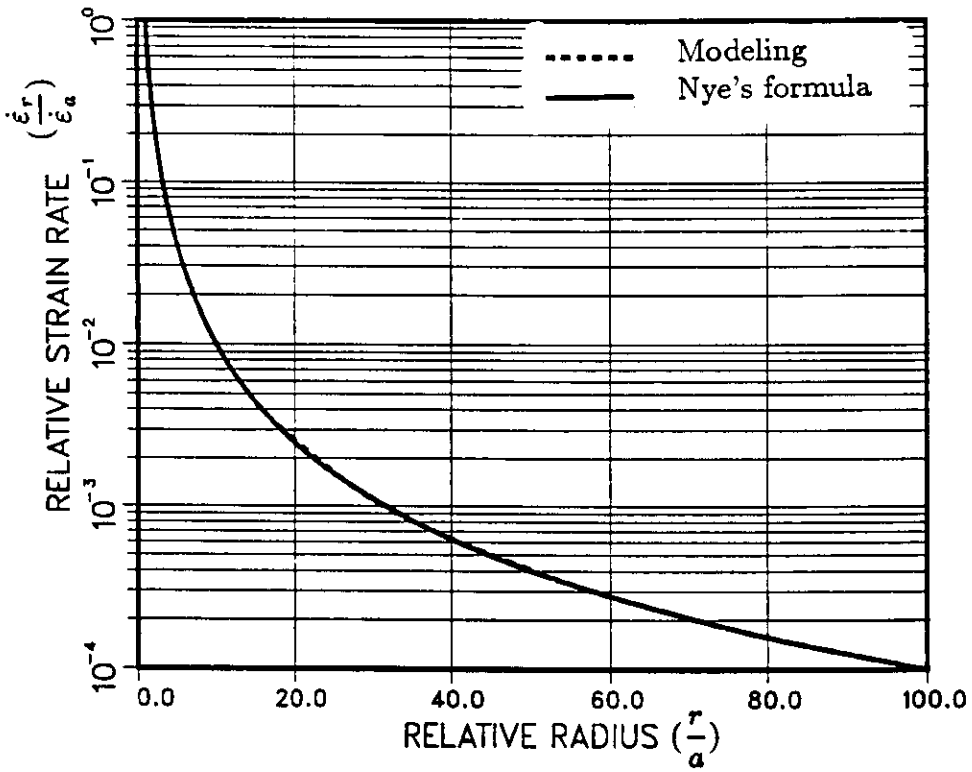

Figure 5. Relative strain rates from modeling and Nye's formula for an idealized ice borehole.

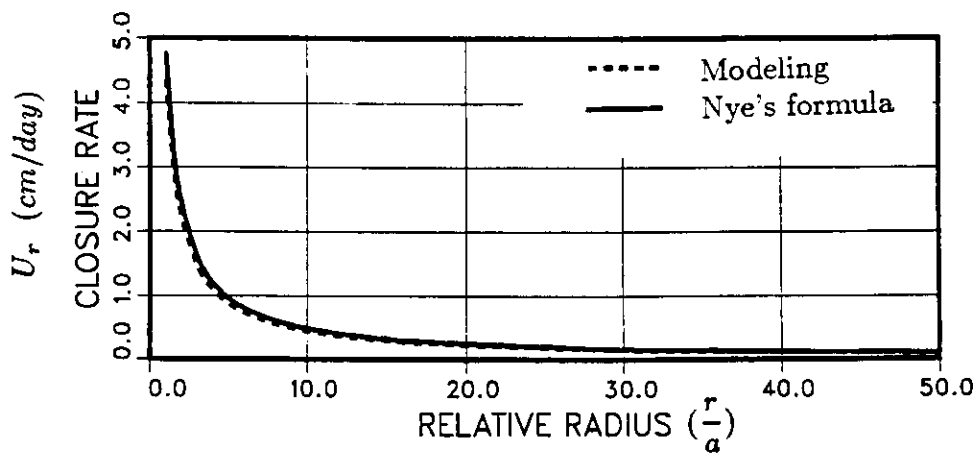

Figure 6. Closure rates from modeling and Nye's formula for an idealized ice borehole.

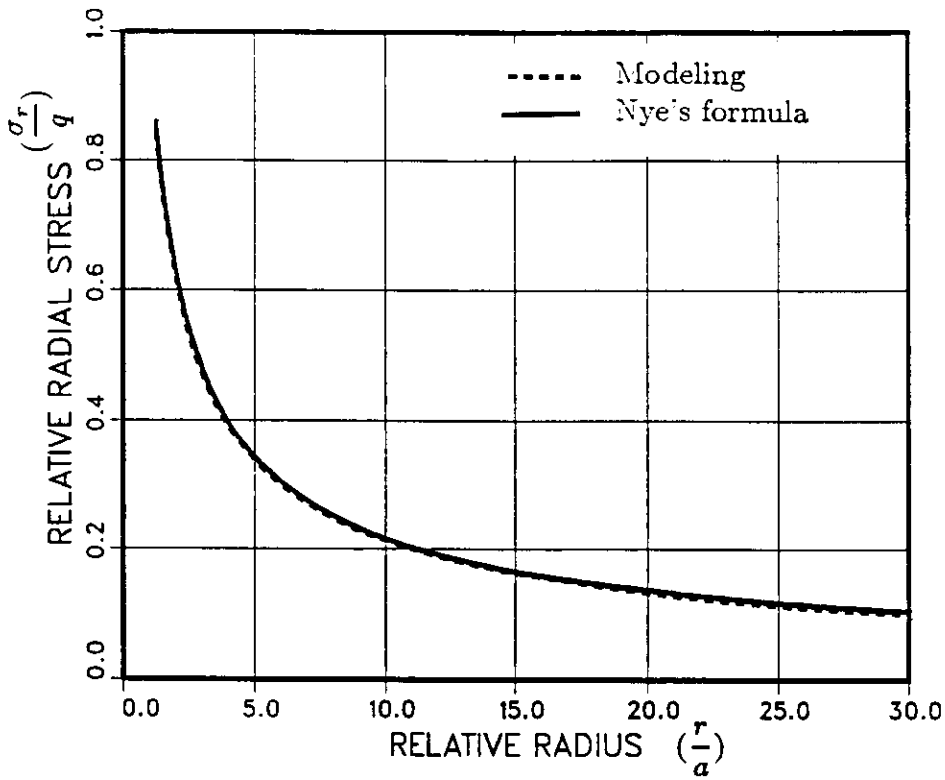

Figure 7. Relative radial stresses from modeling and Nye's formula for an idealized ice borehole.

3.2 Tests with Data from Byrd Station, Antarctica (Dry Hole)

Gow (1963) presented detailed results of measurements in the 309-m deep ice borehole at Byrd Station, Antarctica. The measurements were taken yearly from December 1958 to February 1962. The thickness of the ice sheet at Byrd Station is 2,400 m. The hole had steel casing installed to a depth of 36 m. According to the measurements, closure rates were calculated with diameters measured in December 1958 and January 1961. Measured ice densities were 830 kg/m^3 at 65 m, 900 kg/m^3 at 100 m and 916 kg/m^3 at 309 m. Temperatures were chosen with constant -28.2°C from ice surface to 60-m depth, then linearly decreasing to -28.35°C at 120 m and -28.4°C at 309-m depth.

Because the model results are sensitive to the exponent n in (2.3) and n seems not to be a constant with stress, an attempt was made to establish an empirical relation between n and effective stress τ with the closure rate data from Byrd Station. To fit each data, specific values of n were found by running the model. Then a temporary empirical formula of n was found. By adjusting the parameters of this formula to best fit the data, a final empirical formula was established as (Fig. 8):

$$n = 2.85 + 0.014\tau. \tag{3.4}$$

To be conservative, a modified relation was adopted in standard computations as (Fig. 8):

$$n = 2.9 + 0.01\tau. \tag{3.5}$$

where τ is in bars.

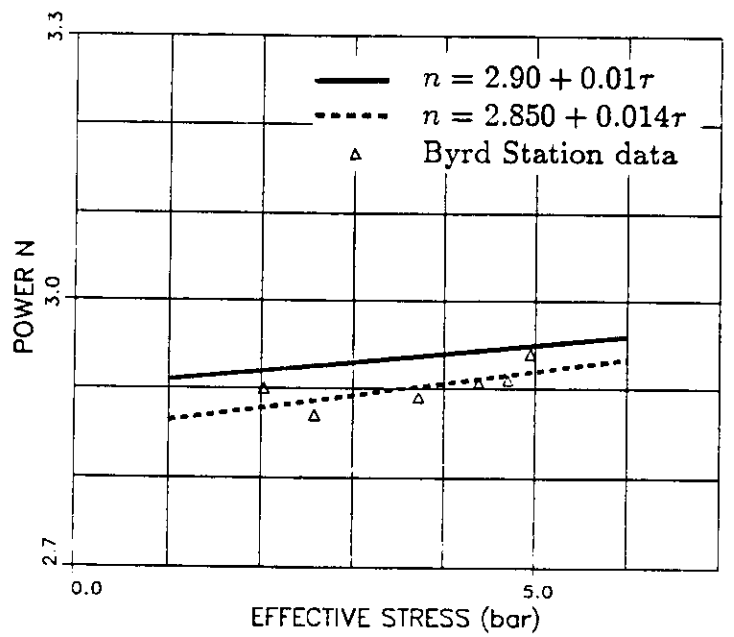

Figure 8. Empirical relation of n and effective stress for dry-ice borehole.

The modeling mesh sketch is shown in Figure 9.

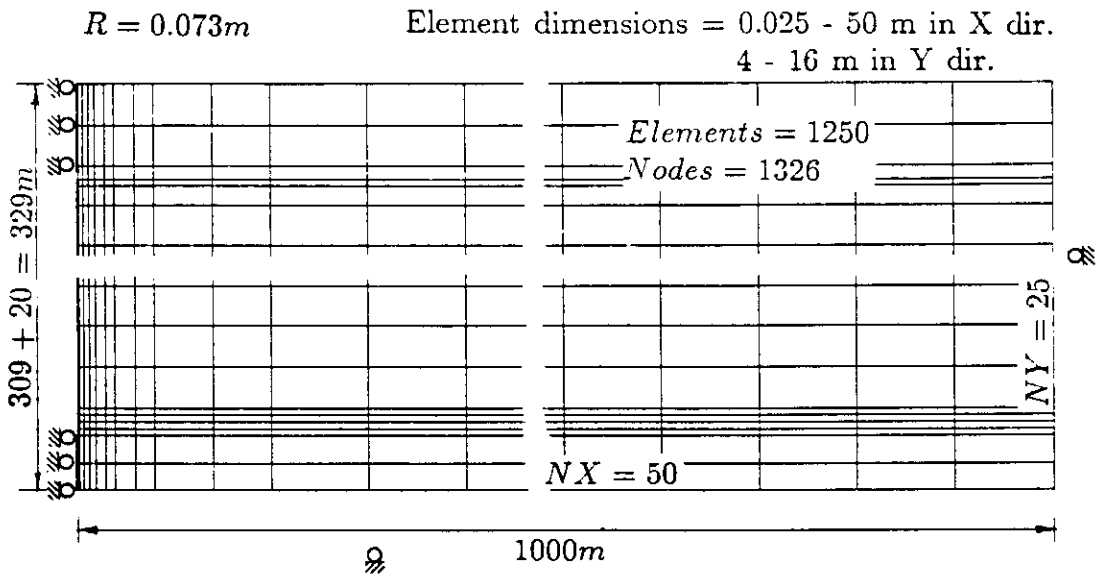

Figure 9. Modeling mesh sketch for a 309-m, dry-ice borehole at Byrd Station, Antarctica (Gow, 1963). The modeled ice depth was extended to 329 m to consider the hole ice base effect. The upper 36 m of steel casing was considered by adding horizontal boundary restrictions. ⫽ denotes boundary restriction perpendicular to the boundary. Hole radius is 0.73 m. Element dimensions are 0.025 to 50 m horizontally and 4 to 16 m vertically.

The modeled ice depth was extended to 329 m to consider the hole ice base effect. The upper 36 m of steel casing was considered by adding horizontal boundary restrictions. ⫽ denotes the boundary restriction perpendicular to the boundary. Hole radius is 0.073 m. Element dimensions are 0.025 to 50 m horizontally and 4 to 16 m vertically.

The model results, together with measurement data and Nye's formula results, are shown in Figure 10. These results show that Nye's formula gives more conservative results in 3 times of model values, and the model can give more accurate values with variable n as a function of effective stress τ (3.5).

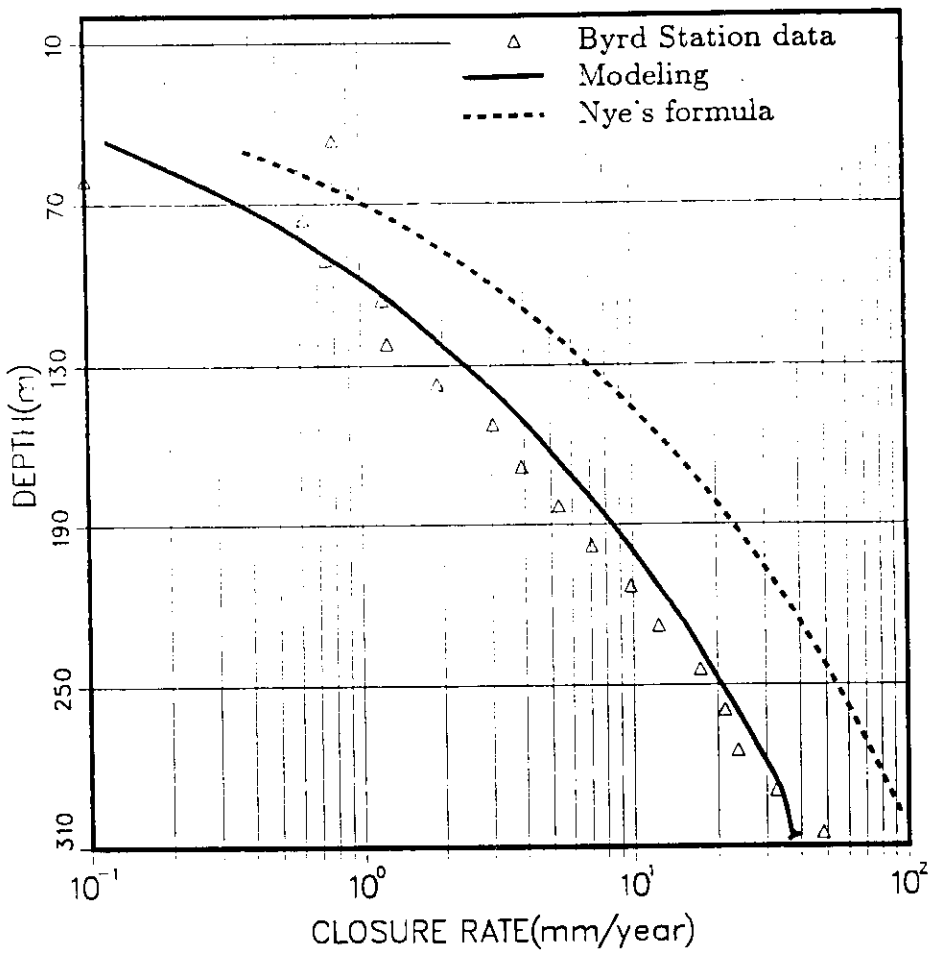

Figure 10. Comparisons of model and Nye's formula in ice borehole closure rates with measurement data from Byrd Station (Gow, 1963).

3.3 Tests with Data from Dye 3, South Greenland (Liquid-Filled Hole)

To examine the model for a liquid-filled ice borehole, data from Dye 3, south Greenland (Hansen and Gundestrup, 1988; Gundestrup and Hansen, 1984) were used. Because significant closure occurred only in the upper 800-m portion, only this portion of the ice borehole was modeled. Ice density of 921 kg/m^3 and temperature of -20° C were used for modeling. Diameter measurements in 1983 and 1985 were used for examining the model. According to the liquid density profile (Hansen and

Gundestrup, 1988), the liquid density was chosen as 903, 985, 990 and 965 kg/m^3 at 120-, 250-, 300- and 800-m levels, respectively, to calculate the liquid pressure. Between these points, the liquid density was assumed to be linearly changing. The upper 120 m was free of liquid, and the hole casing length was 86.8 m.

A feature of a liquid-filled ice borehole is that the effective stress is small near the ice borehole due to ice pressure nearly balanced by liquid pressure. So the exponent n may change in a different way than (3.4), a dry-ice borehole. To examine this a similar method for finding (3.4) was used, and another empirical formula of n was found:

$$n = 2.15 + 0.7\tau. \tag{3.6}$$

which was used by the model to get the best fit with the data from Dye 3. The modeling mesh sketch is shown in Figure 11, and the model results, together with Dye 3 data, are shown in Figure 12. From Figure 12 one can see that the model can still give good results for liquid-filled holes with the empirical formula (3.6). Model results for the Dye 3 hole show that the effective stress near the borehole is in the range of 1 to 1.3 bar.

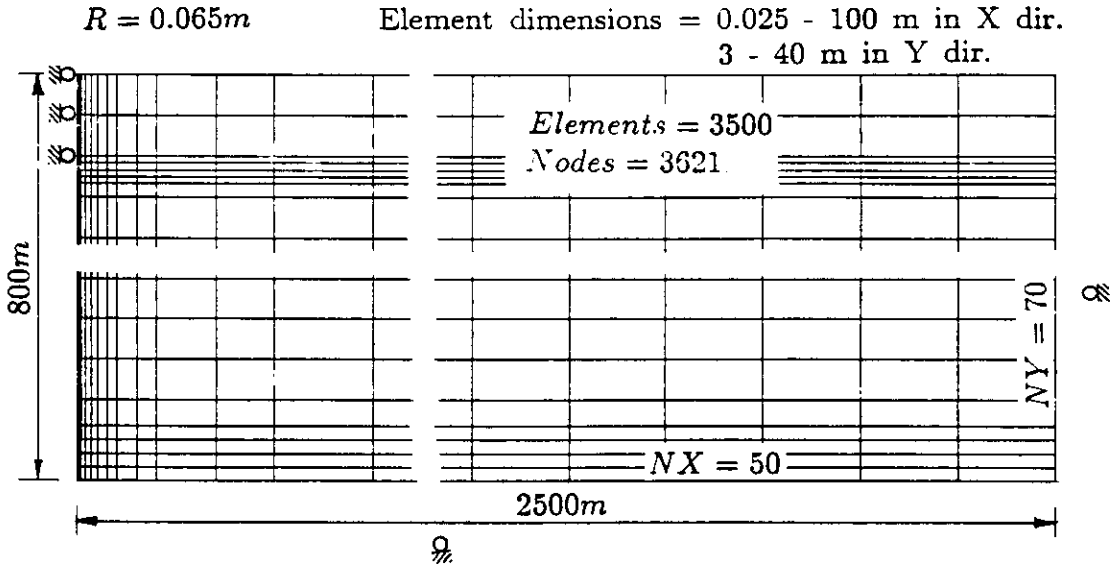

Figure 11. Modeling mesh sketch of a liquid-filled ice borehold at Dye 3, south Greenland (Hansen and Gundestrup, 1988). ⫽ denotes boundary restriction perpendicular to the boundary.

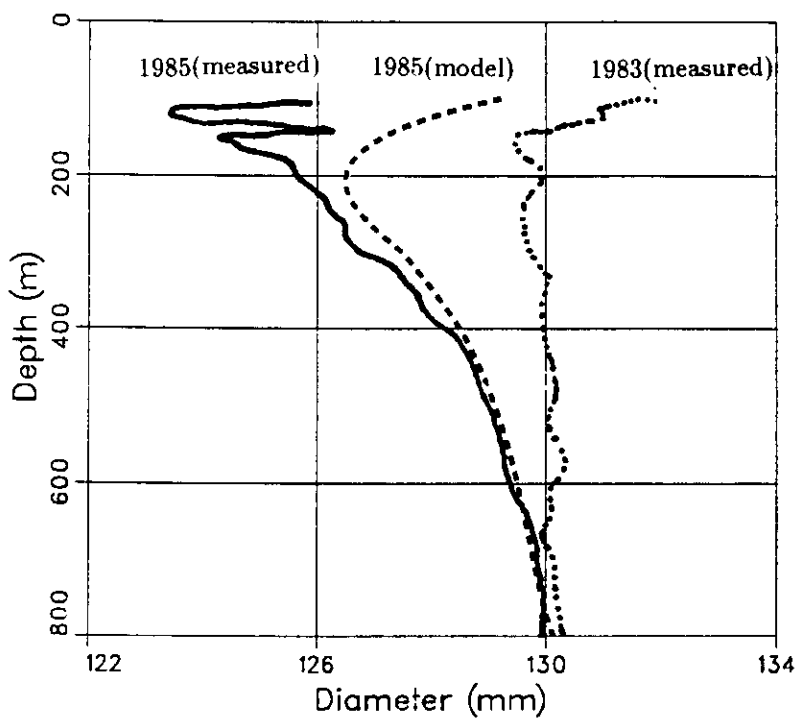

Figure 12. Modeling results and measured diameters of a liquid-filled ice borehole at Dye 3, South Greenland. Part of the figure is from Hanson and Gundestrup (1988). Diameters shown were measured in 1983 and 1985. The original diameter was 130.5 mm.

4. APPLICATION OF THE NUMERICAL MODEL

As an application, the model has been used to calculate the closure rates of an 3,000-m deep ice borehole under different conditions of boundary, temperature and density. The large-scale, compressive ice flow effect on the ice borehole closure has also been examined.

4.1 Standard Computation

To determine the input temperature profile, -35°C surface temperature and -10°C borehole bottom temperatures were chosen, and the profile shape was determined non-linearly by referring to measurements (Figs. 13, 14) and theoretical calculations (Fig. 15). The ice density profile used in the standard computation is linearly distributed with the constant below a 300-m depth. Both the temperature and the density profiles are shown in Figure 16 with solid lines. The model mesh is shown in Figure 17 with dimensions of 3,000 x 8,100 m. The element dimensions vary from 0.025 to 400 m horizontally and 1 to 50 m vertically. Both remote-lateral boundary and bottom boundary are restricted with one-dimension restriction, which means the boundary can only freely move along the boundary direction. This kind of bottom-boundary restriction may be different from the real situation, and its effect will be disscussed in Section 4.2.

Model results for different diameter holes are shown in Figure 18. From this figure one can see the ice borehole closes very quickly at the lower part of the hole, and all holes will close up in one day below the 2,500-m level. These results also verify the relationship that the closure-rate ratio of different diameters of ice boreholes is equal to the diameter ratio.

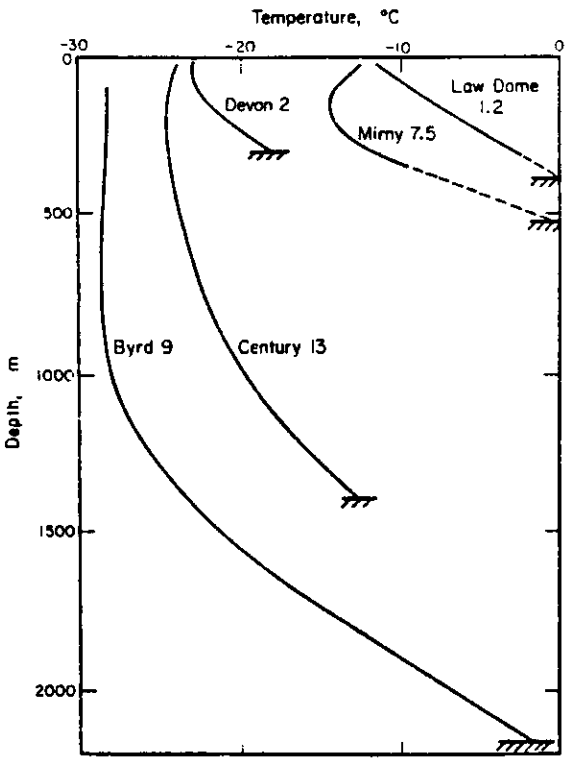

Figure 13. Measured temperature profiles in accumulation areas of polar ice sheets (Paterson, 1981).

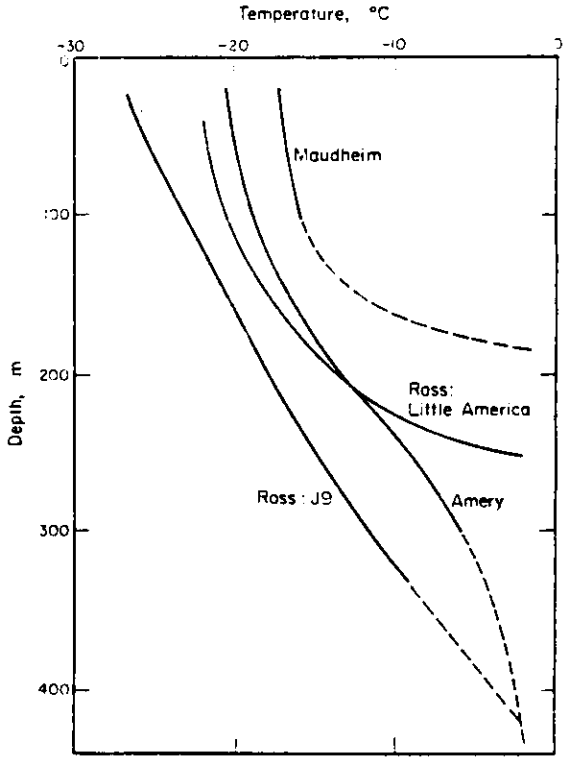

Figure 14. Measured temperature profiles in ice shelves (Paterson, 1981).

4.2 Bottom Boundary Effect on Closure Rate

In standard model computation, the bottom boundary restriction was set only in the direction of perpendicular to the icebed. This means the ice sheet may freely move horizontally. This may be true for the case of the melt water layer between the ice sheet and the flat rockbed. The extremely opposite case is that the bottom ice layer is frozen totally onto the rockbed. This can be simulated with fixed boundary restrictions at the bottom of the ice sheet. Other real bottom boundary conditions are between these two extreme cases. To consider the boundary condition effect on an ice

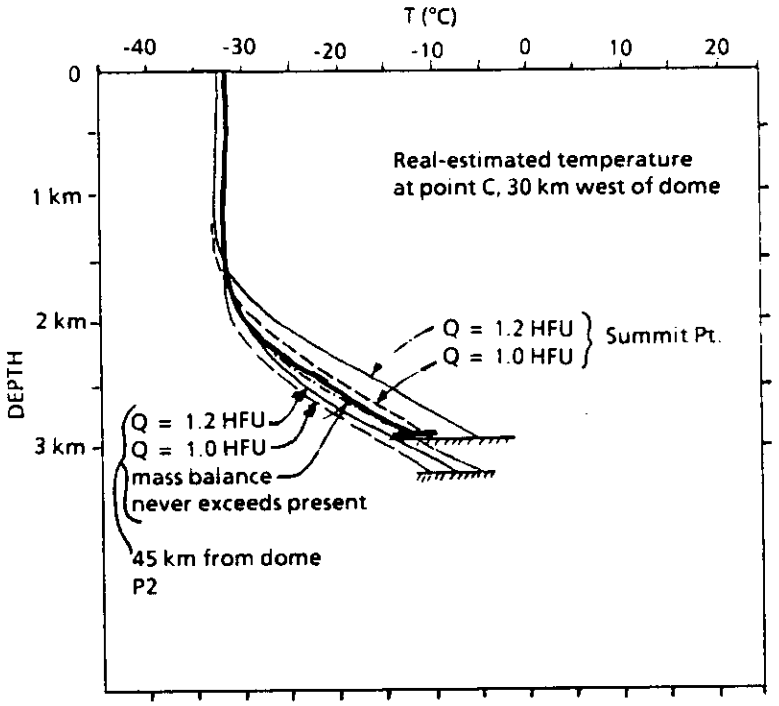

Figure 15. Theoretical estimation of temperature-depth profile at Summit, Greenland (Waddington, 1989).

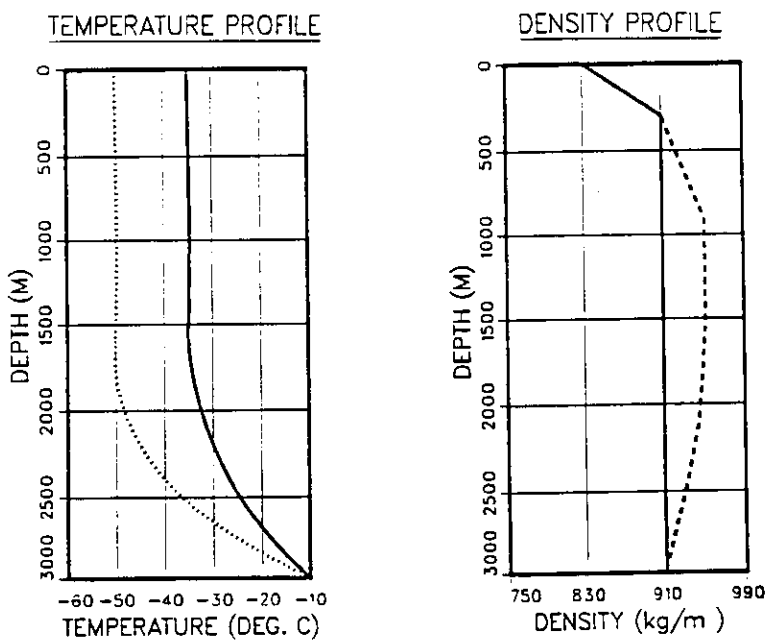

Figure 16. Profiles of temperature and density of ice used in the model. Solid lines represent profiles used in standard computation. Dotted lines and dashed lines are for comparisons of different temperature and density, respectively.

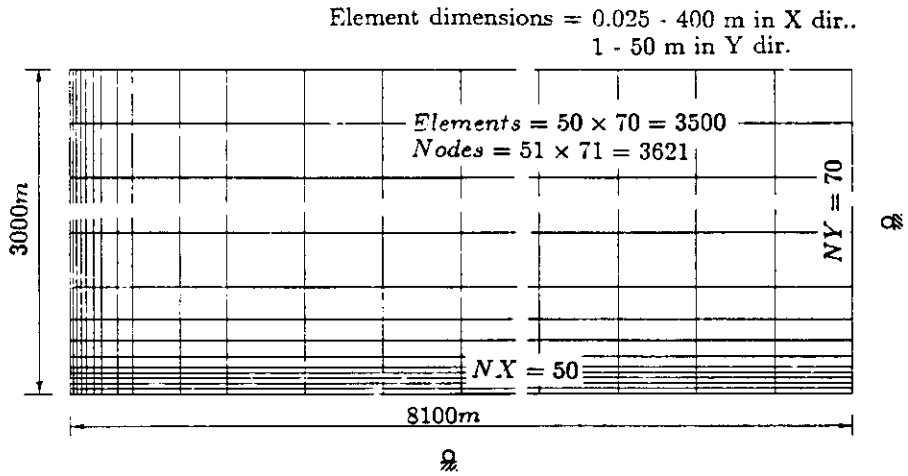

Figure 17. Model mesh sketch (not in scale) for a 3,000-m deep ice borehole. The horizontal dimension of the mesh is 8,100 m. The element dimensions are 0.025-400 m horizontally and 1 to 50 m vertically.

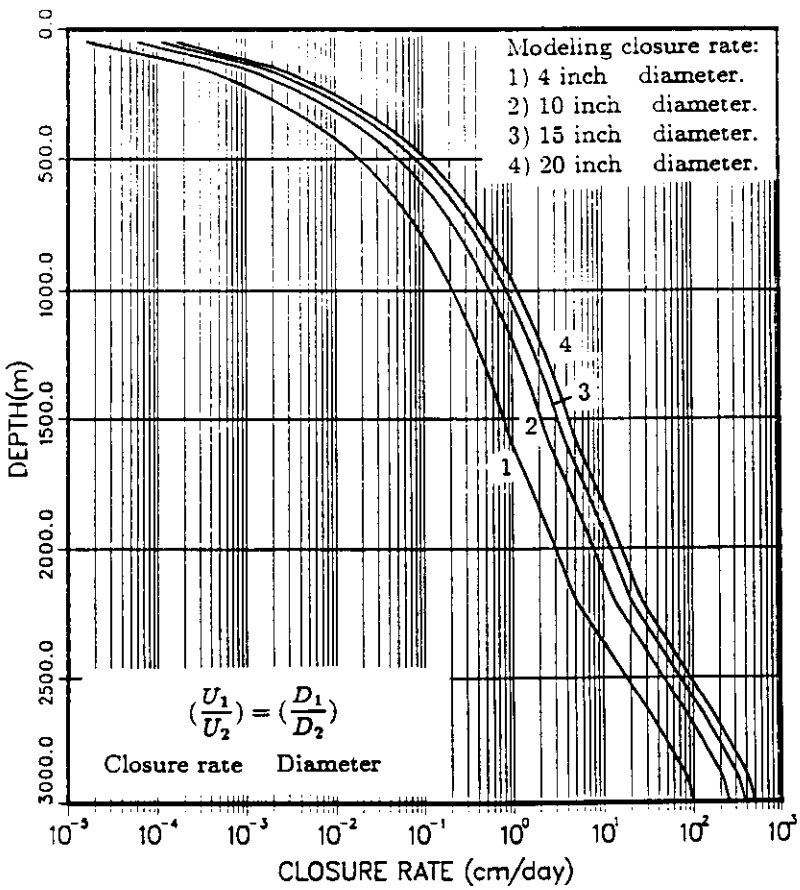

Figure 18. Model results of ice borehole closure rates for different diameter ice boreholes. The diameters are 4, 10, 15 and 20 in, respectively.

borehole closure, three ice boreholes with different depths of 3,000, 2,000 and 1,000 m were chosen as examples. Each borehole was modeled under these two extreme boundary conditions, respectively. The results are shown in Figure 19. From this figure one can see that the effect of boundary conditions on ice borehole closure are the same for different depth ice boreholes. The effect occurs only within the bottom 50- m range, or one can say that the ice borehole boundary layer thickness is 50 m. In this layer the effect decreases quickly within 5 m from the bottom. So on the estimation of whole ice borehole closure, the bottom boundary condition effect is not very important.

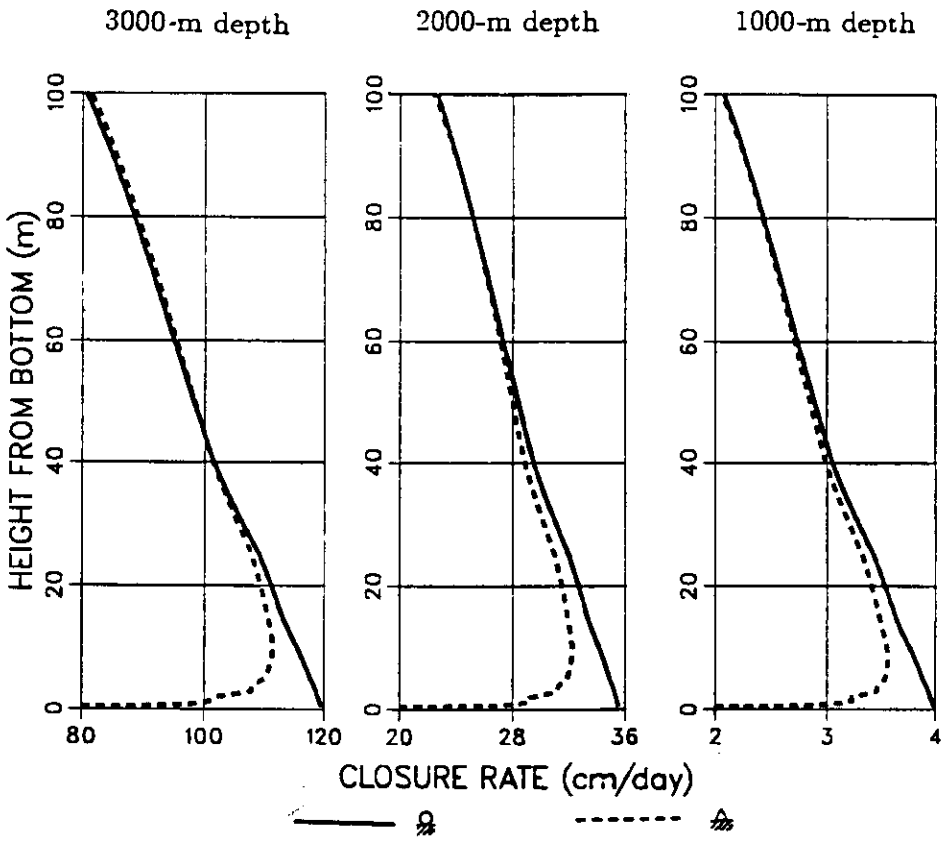

Figure 19. Effects of ice bottom boundary conditions on ice borehole closure rate. Three different depths of ice boreholes are: 3,000, 2,000 and 1,000 m, respectively. Solid lines show closure rate for one-dimension boundary restriction. Dashed lines are for fixed-boundary restriction.

4.3 Temperature and Density Effects

To compare the temperature effect on ice borehole closure rate, another temperature profile with surface temperature of -50°C was chosen to run the model as shown in Figure 16 by the dotted line in Figure 16. The model results are shown by the dotted line in Figure 20. These results show that for a 15°C change in temperature, the closure rate will change 8 times at about the 1,500-m level.

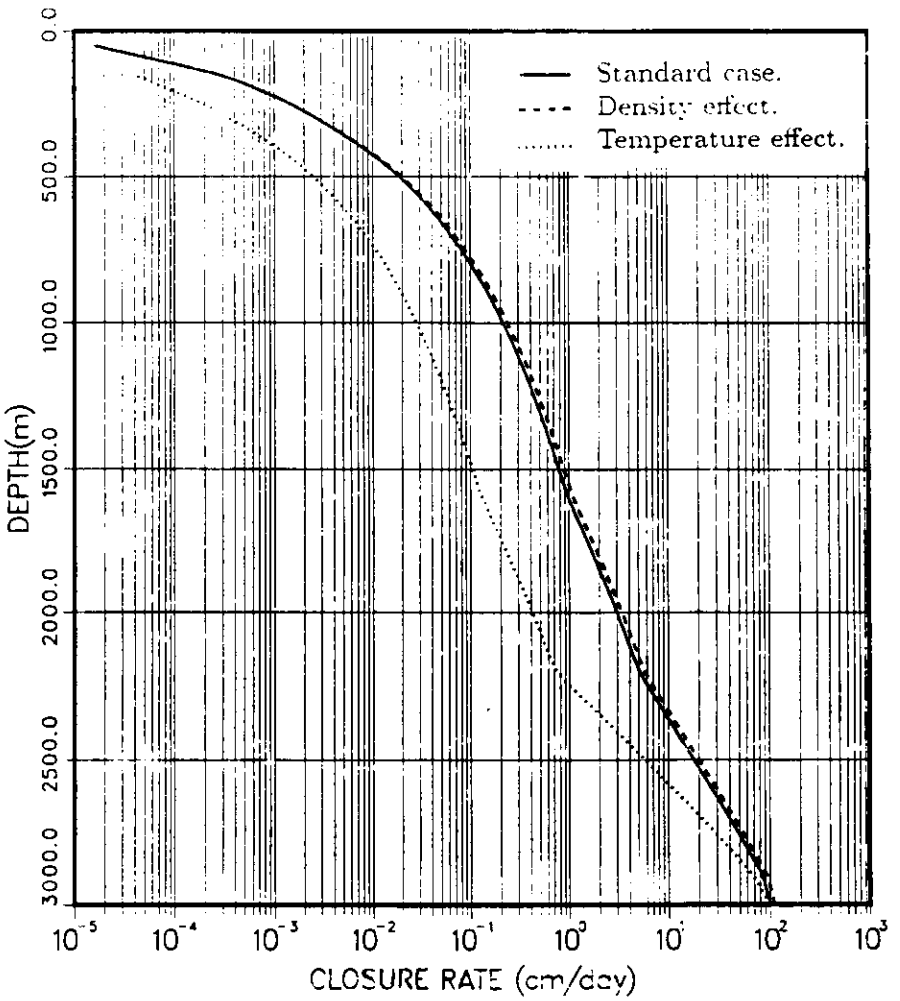

Figure 20. Comparisons of ice temperature and density effects on ice borehole closure rates by modeling. The solid line shows standard model results. The dotted line shows temperature effect. The dashed line shows density effect.

To compare the ice density effect on the ice borehole closure rate, a density profile was calculated (Fig. 16, dashed line) according to an ice density-temperature relation (Alley, 1989; Fig. 21) which is from the measurement of GISP2. The model results are shown with a dashed line in Figure 20. These results show that the effect of ice density on ice borehole closure is relatively small and not very important.

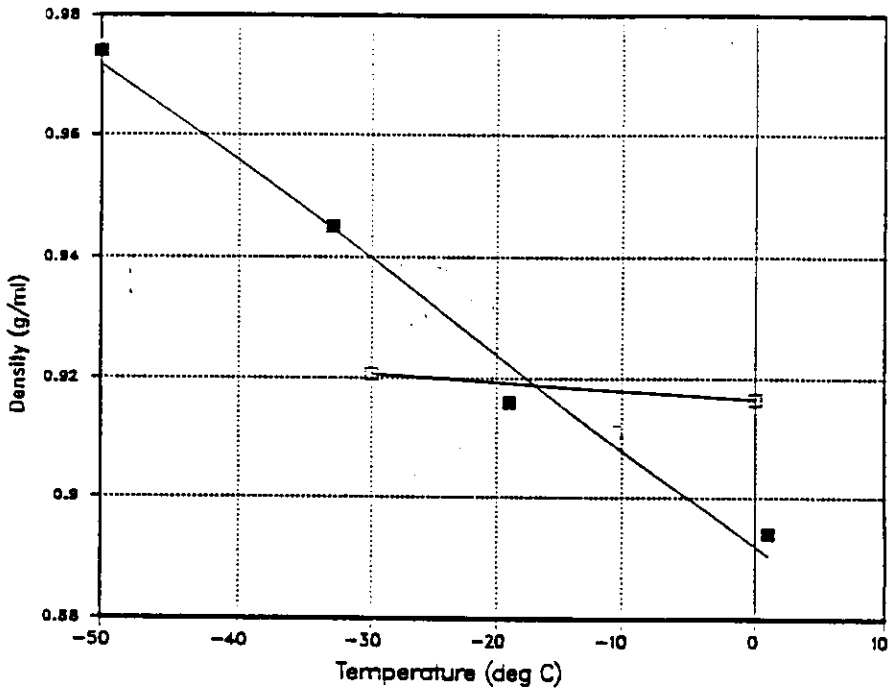

Figure 21. Relationship of ice density and ice temperature (data source: Alley, 1989).

4.4 Ice Flow Effect

Most real ice boreholes are located in ice flows. Except for the inclination effect on the boreholes, the effect of ice flow on borehole closure remains unknown. To examine this effect, a similar numerical model for 2-D viscous incompressible fluid problems was used. The ice borehole closure produced by a compressing ice flow was considered and was treated as a plane symmetric problem. The model mesh is shown

in Figure 22. The borehole diameter was 0.05 m. A relative high ice flow strain rate of $\dot{\varepsilon} = -0.05/a$ was chosen (Paterson, 1981), which is equivalent to relative velocity of $dU = 4.755 \times 10^{-9}$ *m/s* for a 3-m distance. The model results are shown in Figure 23. These results show that the ice borehole closure rate produced by a compressing ice flow is at most in the order of 10^{-2} *m/yr*, which is very small and negligible.

Element dimensions = 0.006 - 0.4 m in X dir.
0.01 - 1 m in Y dir.

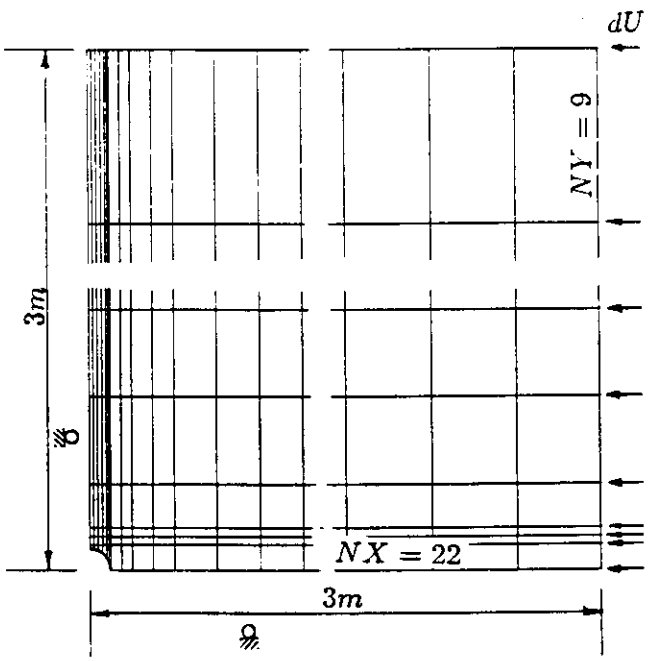

$$dU = 4.755 \times 10^{-9} m/s$$
$$(\dot{\varepsilon} = 0.05/a = 1.585 \times 10^{-9}/s)$$

Figure 22. 2-D model mesh sketch for an ice borehold closure due to compressing ice flow. The relative ice flow velocity is 4.755 x 10^{-9} *m/s*, which is equivalent to a relatively high strain rate of $\dot{\varepsilon} = -0.05/a$ (Paterson, 1981).

On the ice crystal effect on ice deformation, investigations (Russell-Head and Budd, 1979; Hansen and Gundestrup, 1988) show that strong c-axis orientations

usually occur in the deeper ice, and large crystals with multiple maxima fabrics can be found in the lower quarter of the ice sheet. Detailed knowledge remains unknown. To account for the effect of ice crystals on ice borehole closure, a c-axis enhancement factor may be used in the model at the present time. The values of this factor may be chosen according to experience.

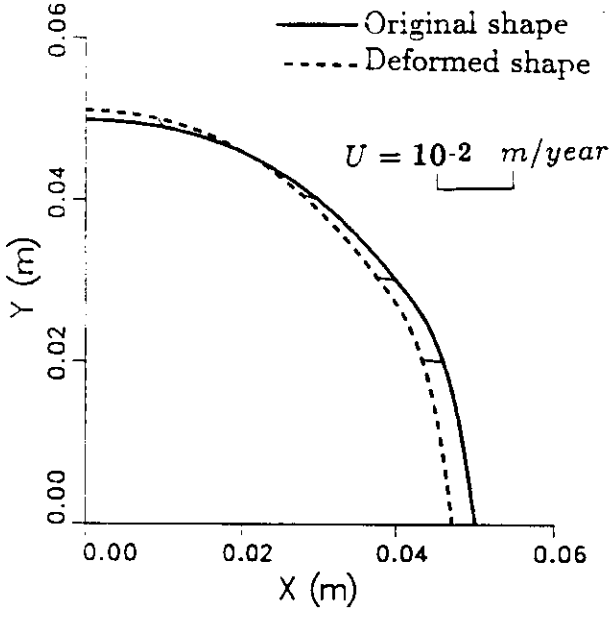

Figure 23. Model results of ice borehole deformation produced by a compressing ice flow. Closure rate is less than 10^{-2} *m/year*.

5. CONCLUSIONS

In the absence of an exact theoretical formula for calculating the ice borehole closure rate, a numerical approach was adopted and a finite element model has been modified. It can be used generally for any ice sheet or glacier ice as long as the local ice conditions are known as input data. Comparisons with Nye's formula and measured data show that the model can give reasonably realistic results as a reference for prospective drill planning.

Test results show that the ice flow power-law exponent n should be considered as a variable of effective stress to get more accurate model results. For a dry-ice borehole a relationship of $n = 2.9 + 0.01\tau$ can be used, and $n = 2.15 + 0.7\tau$ is suitable for liquid-filled ice borehole modeling. The ice bottom boundary effect on the ice borehole closure rate only occurs within 50 m from the bottom. The effect decreases quickly in the first 5 m from the bottom. The temperature effect on the ice borehole closure rate is significant with 8 changes in closure rate at a temperature change of 15°C at about the 1,500-m deep level. The effects of ice density and ice flow on the ice borehole closure are small and negligible.

One thing should be noted. This model should be further modified to consider the ice crystal effect on the ice borehole closure rate once more knowledge becomes available.

6. REFERENCES

Alley, R. 1989. Personal communications.

Cook, R.D., D.S. Malkus and M.E. Plesha. 1989. *Concepts and Applications of Finite Element Analysis.* Third Edition. John Wiley & Sons Press. 630 pp.

Cuvelier, C. and A. Segal. 1986. *Finite Element Methods and Navier-Stokes Equations.* D. Reidel Publishing Company. 483 pp.

Glen, J.W. 1955. The Creep of polycrystalline ice. Proceedings of the Royal Society of London, Serials A, Vol. 228, 519-538.

Gow, A.J. 1963. Results of measurements in the 309-meter bore hole at Byrd Station, Antarctica. *Journal of Glaciology* 4(36):771-784.

Gundestrup, N.S. and B.L. Hansen. 1984. Bore-hole survey at Dye 3, South Greenland. *Journal of Glaciology* 30(106):282-288.

Hansen, B.L. and N.S. Gundestrup. 1988. Resurvey of bore hole at Dye 3, South Greenland. *Journal of Glaciology* 34(117):178-182.

Hutter, K. 1983. *Theoretical Glaciology.* D. Reidel Publishing Company. 510 pp.

Nye, J.F. 1953. The Flow law of ice from measurements in glacier tunnels, Laboratory Experiment and the Jungfranfirn Borehole Experiment. Proceedings of the Royal Society of London, Serials A, Vol. 219, 477-489.

Paterson, W.S.B. 1981. *The Physics of Glaciers.* Second Edition. Pergamon Press. 380 pp.

Rigsby, G.P. 1957. Effect of hydrostatic pressure on velocity of shear deformation of single crystals of ice. Snow Ice and Permafrost Research Establishment. Research Report No. 320.

Russell-Head, D.S. and W.F. Budd. 1979. Ice-sheet flow properties derived from bore-hole shear measurements combined with ice-core studies. *Journal of Glaciology* 24(99):117-130.

Waddington, E.D. 1989. Estimated temperature-depth profile at Summit, Greenland. Personal communication.